



In silico and in vitro screening of licensed antimalarial drugs for repurposing as inhibitors of hepatitis E virus

Borris Rosnay Tietcheu Galani^{1,2} · Vincent Brice Ayissi Owona² · Romeo Joel Guemmogne Temdie³ · Karoline Metzger⁷ · Marie Atsama Amougou^{2,4} · Pascal Dieudonné Djamen Chuisseu⁵ · Arnaud Fondjo Kouam^{2,6} · Marceline Ngounou Djuidje² · Cécile-Marie Aliouat-Denis⁷ · Laurence Cocquerel⁷ · Paul Fewou Moundipa²

Received: 28 December 2020 / Accepted: 16 April 2021

© The Author(s), under exclusive licence to Springer-Verlag GmbH Germany, part of Springer Nature 2021

Abstract

Hepatitis E virus (HEV) infection is emerging in Cameroon and represents one of the most common causes of acute hepatitis and jaundice. Moreover, earlier reports showed evidence of falciparum malaria/HEV coexistence. Although the Sofosbuvir/Ribavirin combination was recently proposed in the treatment of HEV-infected patients, no specific antiviral drug has been approved so far, thereby urging the search for new therapies. Fortunately, drug repurposing offers a good alternative to this end. In this study, we report the in silico and in vitro activities of 8 licensed antimalarial drugs and two anti-hepatitis C virus agents used as references (Sofosbuvir, and Ribavirin), for repurposing as antiviral inhibitors against HEV. Compounds were docked against five HEV-specific targets including the Zinc-binding non-structural protein (6NU9), RNA-dependent RNA polymerase (RdRp), cryoEM structure of HEV VLP, genotype 1 (6LAT), capsid protein ORF-2, genotype 3 (2ZTN), and the E2s domain of genotype 1 (3GGQ) using the iGEMDOCK software and their pharmacokinetic profiles and toxicities were predicted using ADMETlab2.0. Their in vitro effects were also assessed on a gt 3 p6Gluc replicon system using the luciferase reporter assay. The docking results showed that Sofosbuvir had the best binding affinities with 6NU9 (− 98.22 kcal/mol), RdRp (− 113.86 kcal/mol), 2ZTN (− 106.96 kcal/mol), while Ribavirin better collided with 6LAT (− 99.33 kcal/mol). Interestingly, Lumefantrine showed the best affinity with 3GGQ (−106.05 kcal/mol). *N*-desethylamodiaquine and Amodiaquine presented higher binding scores with 6NU9 (− 93.5 and − 89.9 kcal/mol respectively vs − 80.83 kcal/mol), while Lumefantrine had the greatest energies with RdRp (− 102 vs − 84.58), and Pyrimethamine and *N*-desethylamodiaquine had stronger affinities with 2ZTN compared to Ribavirin (− 105.17 and − 102.65 kcal/mol vs − 96.04 kcal/mol). The biological screening demonstrated a significant ($P < 0.001$) antiviral effect on replication with 1 μ M *N*-desethylamodiaquine, the major metabolite of Amodiaquine. However, Lumefantrine showed no effect at the tested concentrations (1, 5, and 10 μ M). The biocomputational analysis of the pharmacokinetic profile of both drugs revealed a low permeability of Lumefantrine and a specific inactivation by CYP3A2 which might partly contribute to the short half-time of this drug. In conclusion, Amodiaquine and Lumefantrine may be good antimalarial drug candidates for repurposing against HEV. Further in vitro and in vivo experiments are necessary to validate these predictions.

Keywords Hepatitis E · HEV · Virtual screening · In vitro screening · Antimalarial drugs

Introduction

Hepatitis E virus (HEV) infection is regarded as a leading cause of acute hepatitis and jaundice in the world. According to previous estimates, over 20 million infections are recorded annually, with about 3.3 million symptomatic cases

(Rein et al. 2012). In 2015, the World Health Organization (WHO), reported about 44,000 deaths due to HEV which represents 3.3% of the mortality attributable to all forms of viral hepatitis (WHO 2020). Other studies indicated a higher annual incidence, with 56,600 (Lozano et al. 1990) and even 70,000 deaths/year (Navaneethan et al. 2008).

HEV is a quasi-enveloped positive-sense RNA virus, member of the *Hepeviridae* family within the *Orthohepevirus* genus. Its genome is made of a singled-strand RNA of about 7.2 kilobases in length which possess three major

✉ Borris Rosnay Tietcheu Galani
b.tietcheu@gmail.com; borris.galani@univ-ndere.cm

Extended author information available on the last page of the article

and conserved open reading frames (ORFs). The ORF-1 encodes a non-structural polyprotein exerting methyltransferase, papain-like cysteine proteases, helicase, and RNA-dependent RNA-polymerase (RdRp) activities needed for the viral replication. ORF-2 encodes the viral capsid protein, and ORF-3, a small phosphoprotein palmitoylated (Gouttenoire et al. 2018) of ~ 13 kDa involved in virion morphogenesis and release (Kenney and Meng 2019). Recently, a novel ORF-4, positioned within the ORF-1 sequence, has been identified in genotype (gt) 1 HEV strains only, and ORF-4 protein was found to stimulate the viral polymerase activity (Nair et al. 2016). To date, 8 genotypes at least have been described (Nimgaonkar et al. 2018), of which gt 1 and 2 known to only infect humans (Smith et al. 2014), while gt 3 and gt 4 fewer pathogens, are zoonotic and can both infect animals and humans (Doceul et al. 2016).

In developing countries, hepatitis E occurs as large epidemics due to poor sanitation, and pregnant women in this context are associated with high mortality rates (about 33%) (Donnelly et al. 2017). Moreover, some sporadic cases of coinfection with malaria have been reported (Aslam 2017; Turner and Ch'ng 2008). In Cameroon, proofs of HEV circulation have been documented. Amougou et al., in a prospective case–control study found a high prevalence of HEV in Cameroonian patients with hepatocellular carcinoma (HCC) compared to non-HCC patients with chronic liver disease (41.8% vs 12.6%) (Amougou et al. 2017). A report by another group indicated the presence of HEV serologic markers in HIV-infected patients, pregnant women, and the elderly population (Modiyinji et al. 2019). A prevalence of 6.7% and 12.2% was reported for anti-HEV immunoglobulins IgG and IgM respectively in HIV-infected patients in Yaoundé (Wilson et al. 2020). The first studies on the molecular characterization of human HEV isolates collected in infected patients from North Cameroon revealed the occurrence of gt 1 and 3 (Modiyinji et al. 2020), confirming thereby the transmission of zoonotic strains previously identified in pigs (Modiyinji et al. 2018). Therefore, the search for efficient antivirals is needed.

Actually, there is no specific cure for HEV infection. Recently, the HEV 239 vaccine, called Hecolin was approved in China but is still unavailable for other countries (Nan et al. 2018). Therefore, efforts are more concentrated on the search for new antiviral inhibitors. The development of anti-HEV drugs has been slowed down, for a long time, due to difficulties to purify the viral polymerase and replicating effectively HEV in cell culture. The current treatments include the administration of the ribavirin (RBV)/pegylated interferon-alpha combination which clears the virus, at 80%, but the multiple side effects, failure in achieving a sustained virological response, and the emergence of viral resistant-mutants, increasingly prompted the search for alternative therapies (Kinast et al. 2019). Drug repurposing or

repositioning is an alternative approach consisting to reuse existing drugs to treat another pathology than the primary indication. This approach could be an efficient way to overcome the time limitation research and development needed to design a therapeutic drug against HEV. A clear advantage of the repositioned drug over traditional drug development is that since the repositioned drug has already passed a significant number of tests including clinical trials, its safety is known, and the risk of failure is reduced (Kinast et al. 2019). Thanks to this advantage, drug repurposing has retained the attention of the scientific community over this last decade especially in the field of viral diseases. For example, Sofosbuvir, an antiviral agent approved against hepatitis C was recently found efficient in inhibiting HEV replication in cell culture (Thi et al. 2016) and during clinical studies (Fraga et al. 2019), particularly when combined to RBV. Since HEV infection has been also reported in malaria patients, repurposing antimalarial drugs against hepatitis E could be viewed as a promising strategy. Animal models usually raised ethical concerns as well as translational questions of research findings to humans. Therefore, human-based computer models appear as good alternatives as many of them demonstrated higher accuracy than animal models in clinical risk prediction and pharmacological evaluation (Passini et al. 2017). Previous works recently highlighted the *in silico* antiviral potential of antimalarial drugs against the coronavirus disease 2019 (COVID-19) (Sachdeva et al. 2020). In this study, we report new findings on the *in silico* activity of eight licensed antimalarial drugs against different HEV proteins.

Material and Methods

Drugs screened for repurposing activities

We examined eight approved antimalarial drugs including Amodiaquine, Artemisinin, Chloroquine, Hydroxychloroquine, Lumefantrine, Mefloquine, Quinine, and Pyrimethamin for their repurposing potential against HEV infection. Sofosbuvir and Ribavirin, two antiviral drugs used against hepatitis C were selected as controls to compare interaction between antimalarial and antiviral drugs. The 2D structures of all these drugs is shown in Fig. 1.

Molecular docking and evaluation of the ADMET properties

The 3D structures of the tested compounds were obtained from the PubChem database in SDF format. Files were then transformed into MDL MOL files with Open Babel. The 3D structures of viral proteins were retrieved from the protein data bank (PDB) repository. These include: the Zinc-binding

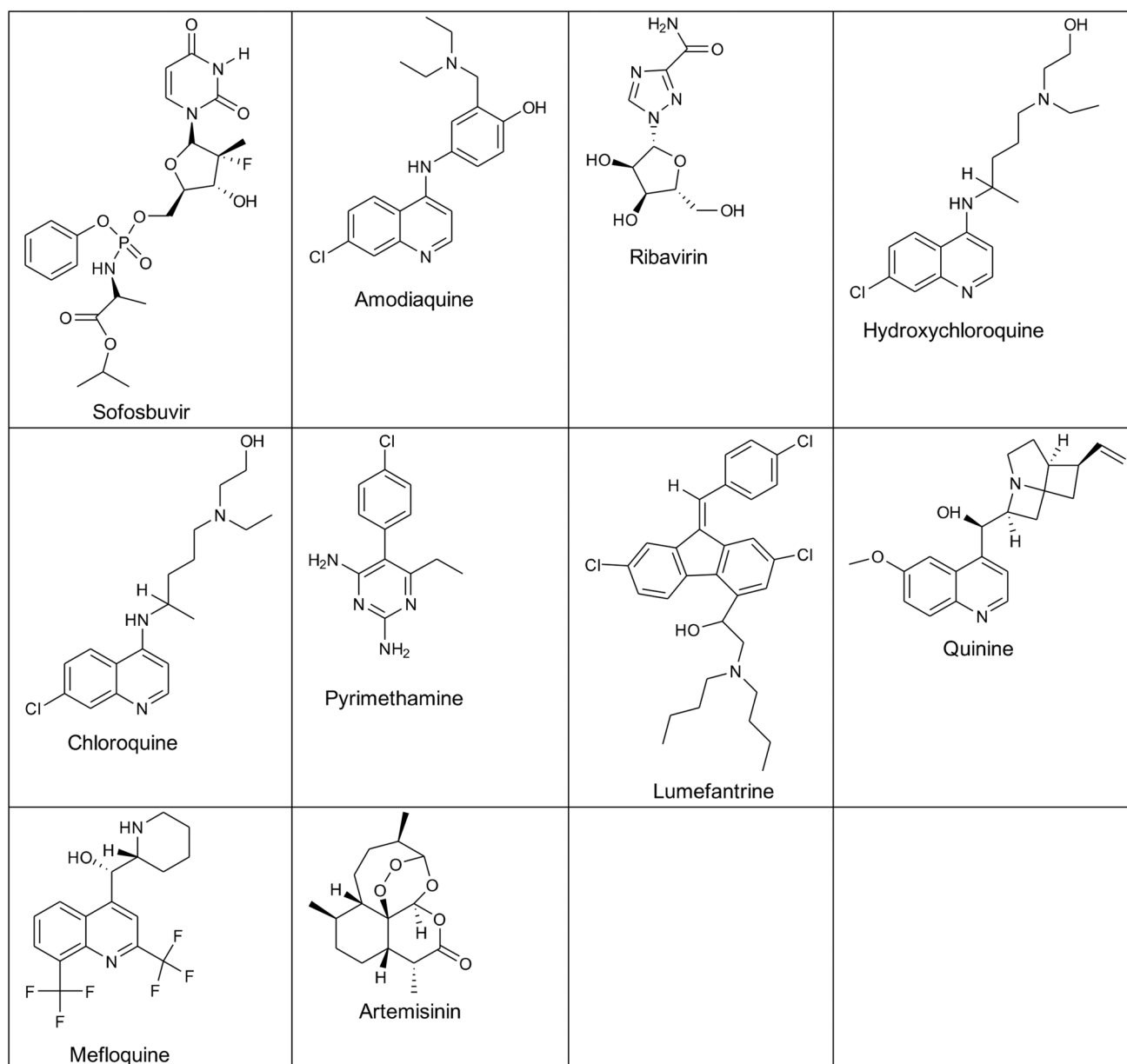


Fig. 1 2D structures of the docked antimalarial and anti-hepatitis C drugs

non-structural protein (PDB ID: 6NU9), the cryoEM structure of HEV VLP, genotype 1 (PDB ID: 6LAT), the capsid protein ORF-2, genotype 3 (PDB ID: 2ZTN), and the capsid protein E2s domain, genotype 1 (PDB ID: 3GGQ). The FASTA sequence of the RNA-dependent RNA polymerase fragment of HEV was obtained from Uniprot (UniProt ID: A0A2Z4GU00_HEV) and a homology modeling was done using the SWISS-MODEL program. Compounds were docked against each PDB file using the drug screening mode of the iGEMDOCK software (version 2.1) provided by BioXGEM lab. For each docking, a total of 30 conformers was used with the full set of ten compounds.

The below parameters were used: population size = 200, generation = 70, and number of solutions = 3. The post-analysis method helped us to visualize and determine drug interactions. The docking scores of the predicted poses were calculated as the total energy in the binding site:

$$\text{Fitness} = \text{VdW} + \text{Hbond} + \text{Elec.}$$

with the VdW term referring to van der Waal energy. Hbond and Elec terms are hydrogen bonding energy and electrostatic energy, respectively. Fully description of the iGEMDOCK scoring function is presented by Yang and Shen (Yang and Shen 2005). Protein–ligand complexes were visualized using RasMol and UCSF Chimera 1.14 and

the pharmacological interactions were analyzed using the IGMDOCK post-analysis tool to detect interacting amino acids.

Besides, the pharmacokinetic properties of the different drugs were predicted using ADMETlab2.0, a free web platform available at <http://admet.scbdd.com/> and supported by the CBDD group from the Xiangya School of Pharmaceutical Sciences & Central South University. This web interface systematically evaluates absorption, distribution, metabolism, excretion (ADME) properties, and various toxicities (T) of the chemical compounds based on a comprehensive collected database consisting of 288,967 entries (Dong et al. 2018). Absorption was evaluated by estimating Caco-2 and MDCK permeabilities, the interactions as substrate or inhibitor of p-glycoprotein (P-gp), the human oral bioavailability 30% ($F_{30\%}$), and human gastrointestinal absorption (HGI). Parameters of distribution included the blood–brain barrier (BBB) penetration, plasma protein binding (PPB), and volume distribution (VD), while the metabolism consisted of analyzing the interaction with the cytochromes P450 isoforms (CYP). For the excretion, the clearance and half-life ($T_{1/2}$) of drugs were estimated. For the toxicological aspect, the heart effect was determined by measuring the ability to behave as hERG blockers. Human hepatotoxicity (H-HT), carcinogenicity, and respiratory toxicity were also examined.

RdRp model building with SWISS-MODEL template library

Template search has been conducted with BLAST and HHblits using the SWISS-MODEL template library (SMTL), (last update: 2021–02–03, last included PDB release: 2021–01–29). The target sequence was searched with BLAST against the primary amino acid sequence contained in the SMTL. An initial HHblits profile has been built using the procedure as previously reported (Steinegger et al. 2019) followed by 1 iteration of HHblits against Uniclust30 (Mirdita et al. 2016). The obtained profile has then be searched against all profiles of the SMTL. A total of 150 templates were found. The porcine Aichi virus polymerase (PDB ID: 6R1I) which exhibited the best sequence identity (23.64%) was used as a suitable template for HEV_RdRp modeling. Models have been built based on the target-template alignment using ProMod3. Coordinates that are conserved between the target and the template were copied from the template to the model. Insertions and deletions were remodeled using a fragment library. Sidechains were then rebuilt. Finally, the geometry of the resulting model was regularized by using a force field. In case of failure of the loop modeling with ProMod3, an alternative model was built with PROMOD-II (Guex et al. 2009). The global and per-residue model quality has been assessed using the QMEAN scoring function (Studer et al.

2020). The oligomeric state conservation was appreciated using the GMQE score which estimates the accuracy of the tertiary structure of the resulting model. The modeled protein was validated by drawing the Ramachandran plot (<https://swissmodel.expasy.org/assess/XXVhRp/02>). The phi-psi angles of 92.45% of amino acids were found in the favored regions. The RdRp model was also checked in the ProSA-web server. The 3D analysis revealed that the model had a Z score of -0.72 (suppl. Figure 1).

Replicon

The HEV p6GLuc replicon was constructed from the HEV genotype 3 Kernow-C1 p6 strain (Accession number JQ679013.1) and was obtained from Dr. S. Emerson, NIAID, NIH, Bethesda, USA. This replicon possesses a *Gaussia Luciferase* reporter gene that substitutes the 5' part of the ORF2 gene and most part of the ORF3 gene (Emerson et al. 2013; Shukla et al. 2012). Thus, the p6GLuc replicon does not form viral particles and cannot infect neighboring cells and the *Gaussia Luciferase* gene is transcribed by the viral replicase ORF1. Therefore, the luciferase activity is directly proportional to the replication activity of the HEV p6GLuc replicon. It is also convenient for kinetics as the Luciferase is secreted into the cell supernatant. A p6GLuc GAD mutant replicon in which the ORF1 polymerase active site GDD was mutated to GAD to prevent any replication was used as a negative control (Emerson et al. 2013).

Capped mRNA synthesis

First, the plasmid DNA of the p6GLuc and p6GLuc GAD mutant replicons were linearized using the restriction enzyme MluI. The restriction digestion was conducted for 2 h at 37 °C in 100µL reaction mix as follows: 25 µg plasmid DNA, 10µL Cutsmart buffer 10x, 62.5µL RNase free water and 2.5µL MluI (NEB, 10,000 units/mL). Next, the DNA was separated from protein by adding 50µL sodium acetate (3 M, pH 5.5) and 500µL chloroform/isoamyl alcohol (96 Vol.: 4 Vol.) and centrifuging at 14,000 rpm for 4 min. The supernatant was transferred, mixed with 700µL ethanol absolute and incubated at -20 °C for 20 min. The DNA pellet was vortexed and centrifuged at 14,000 rpm. The pellet was washed twice with 70% ethanol, dried and suspended in 25 µL RNase free water. The capped mRNA of the p6GLuc replicons were synthesized by in-vitro transcription of the MluI-linearized DNA according to the mMMESSAGE mMACHINE kit (Ambion) and stored at -80 °C before electroporation in PLC3 cells.

Cell culture, electroporation and treatments

PLC3 cells are a subclone of the PLC/PRF/5 (CRL-8024) hepatoma cells and were characterized as the productive cell line for HEV particles by Montpellier et al. (2018). PLC3 cells were cultured in Dulbecco's modified Eagle's medium (DMEM) containing 10% FBS and 1% non-essential amino acids (DMEM complete). The p6GLuc and p6GLuc GAD mutant replicons were electroporated in PLC3 cells as follows. After trypsinization, cells were resuspended in DMEM complete medium and washed twice in Opti-MEM medium. Three million cells were electroporated with 10 µg of RNA of the HEV replicon constructs and resuspended in 6 mL DMEM complete medium.

Compound treatment

The compounds Lumefantrine, Amodiaquine and N-desethylamodiaquine (Sigma Aldrich, Schnellendorf, Germany) were diluted in DMSO at a stock concentration of 50 mM. Sofosbuvir, diluted at the same concentration in DMSO, served as a control of the inhibition of HEV replication. It acts as a chain terminator during replication and its antiviral potential was demonstrated using a genotype 3 replicon in Huh7 and HepG2 cells (Dao Thi et al. 2016). The electroporated cells were seeded in 96-well plates (20,000 cells/well) and incubated for 5 days at 37 °C in a humidified atmosphere containing 5% CO₂. The compounds were added at different concentrations to the electroporated PLC3 cells. The final concentration of DMSO per well was 0.05% or lower. The supernatants (10 µL) were sampled at 1, 3, 4 and 5 days post-electroporation (dpe) and stored at -20 °C until luminescence reading.

Luciferase assay

The supernatants were thawed and centrifuged at 14,000 rpm for 5 min to remove any cell debris. Next, the samples were diluted 1:100 in 1X passive lysis buffer (Promega) and 5 µL were transferred into a white Nunc 96-well plate. At 1 second after injection of 20 µL of the substrate solution (Renilla Luciferase Assay System, Promega), relative light units (RLUs) were acquired on a Centro Luminometer during 1 s. Experiments were repeated three times for each tested compound. Means of RLUs acquired from 3 well at each time point are calculated. The results are expressed as replication folds normalized to day 1 post-electroporation.

Cell viability Assay

Cell viability was determined by using the CellTiter 96@ AQ_{ueous} One Solution Cell Proliferation Assay (MTS) by Promega. After aspirating the cell supernatant of the plated

cells, 100 µL of the 1× MTS solution diluted in DMEM medium was added to each well. After 1–2 h, the absorbance was read at 490 nm by a Microplate Reader (BioTek).

Statistical analysis

Data were presented as mean ± standard deviation (SD) of three sets of experiments. Statistical analysis was carried out using the GraphPad Prism 5.0 software for windows. The comparison of means was performed using a two-way analysis of variance (ANOVA) followed by Bonferroni's post hoc tests. Differences were considered significant when $P < 0.05$.

Results

Interaction analysis of drugs with the Zinc-binding non-structural protein (6NU9)

As shown by Table 1, docking results revealed that Sofosbuvir has the greatest binding affinity with 6NU9 with a fitness value of -98.22 kcal/mol, followed by N-desethylamodiaquine (-93.5 kcal/mol), Amodiaquine (-89.9 kcal/mol), and Lumefantrine (-86.01 kcal/mol). The binding scores of these antimalarial drugs were greater than that of Ribavirin (-80.83 kcal/mol). The top docked poses showed common van der Waal interactions with Gln91, Ser92, Thr102, Tyr103, Ala104, Glu111, Arg113, Arg122, and the binding site of 6NU9 (Fig. 2a–c). Interestingly, N-desethylamodiaquine and Sofosbuvir both formed 4 hydrogen bonds including one common H-bond with Thr 102 which seems to be an important amino acid residue in the active site. However, Lumefantrine and other ligands, lacked such polar interactions.

Docking results of drugs with the RNA-dependent RNA polymerase of HEV

The RNA-dependent RNA polymerase (RdRp) of HEV is a small proteic fragment of 90 amino acid residues released after processing of the non-structural ORF-1 polyprotein and which acts as a key enzyme of the replication process. Docking results showed higher binding scores of RdRp with Sofosbuvir (-113.86 kcal/mol), followed by Lumefantrine (-102 kcal/mol), and Amodiaquine (-93.91 kcal/mol). However, the affinity of these antimalarial drugs were greater than that of Ribavirin (-84.58 kcal/mol) (Table 1). The docking poses of these drugs (Figs. 2e, f) were stabilized by the same hydrophobic interactions involving 9 amino acid residues (Trp30, Lys31, Lys32, His33, Glu 36, Gly 38, Trp42, Asn43 and Trp46) indicating therefore similar binding modes. However, Lumefantrine showed

Table 1 Docking scores of drugs on HEV protease (6NU9) and polymerase (RdRp)

Ligand	Energy ^a (kcal/mol)	VDW ^b (kcal/mol)	Hbond ^c (kcal/mol)	Elec ^d (kcal/mol)
Zn-binding non structural protein of HEV (6NU9)				
Amodiaquine	- 89.9	- 76.56	- 12.84	0
<i>N</i> -desethylamodiaquine	- 93.5	- 77.03	- 16.46	0
Lumefantrine	- 86.01	- 86.01	0	0
Chloroquine	- 81.08	- 73.87	- 7.2	0
Mefloquine	- 76.42	- 63.61	- 12.81	0
Hydroxychloroquine	- 76.37	- 60.94	- 15.43	0
Quinine	- 75.64	- 60.63	- 15.01	0
Pyrimethamine	- 63.59	- 50.66	- 12.93	0
Artemisinin	- 63.44	- 50.7	- 12.74	0
Sofosbuvir	- 98.22	- 78.04	- 20.17	0
Ribavirin	- 80.83	- 53.13	- 27.71	0
RNA-dependent RNA polymerase of HEV				
Amodiaquine	- 93.91	- 89.25	- 4.67	0
<i>N</i> -desethylamodiaquine	- 86.02	- 80.02	- 6	0
Lumefantrine	- 102	- 102	0	0
Chloroquine	- 86.63	- 86.63	0	0
Mefloquine	- 86.76	- 77.71	- 9.05	0
Hydroxychloroquine	- 83.02	- 77.53	- 5.49	0
Quinine	- 84.11	- 75.74	- 8.38	0
Pyrimethamine	- 73.88	- 57.57	- 16.31	0
Artemisinin	- 74.05	- 52.27	- 21.79	0
Sofosbuvir	- 113.86	- 101.34	- 12.52	0
Ribavirin	- 84.58	- 54.12	- 30.46	0

additionally vdW contacts with Phe29 and no H-bond, while Sofosbuvir exhibited H-bonds with 3 amino acid residues (Lys31, Trp42, Trp46) and Amodiaquine with only one (Lys32) (Table 3).

Interaction analysis of drugs with the HEV capsid proteins

HEV capsid proteins are proteins essential for viral entry and assembly. Compounds that inhibit or strongly bind to these molecules could interfere with these processes.

Effect on the HEV VLP CryoEM structure, genotype 1(6LAT)

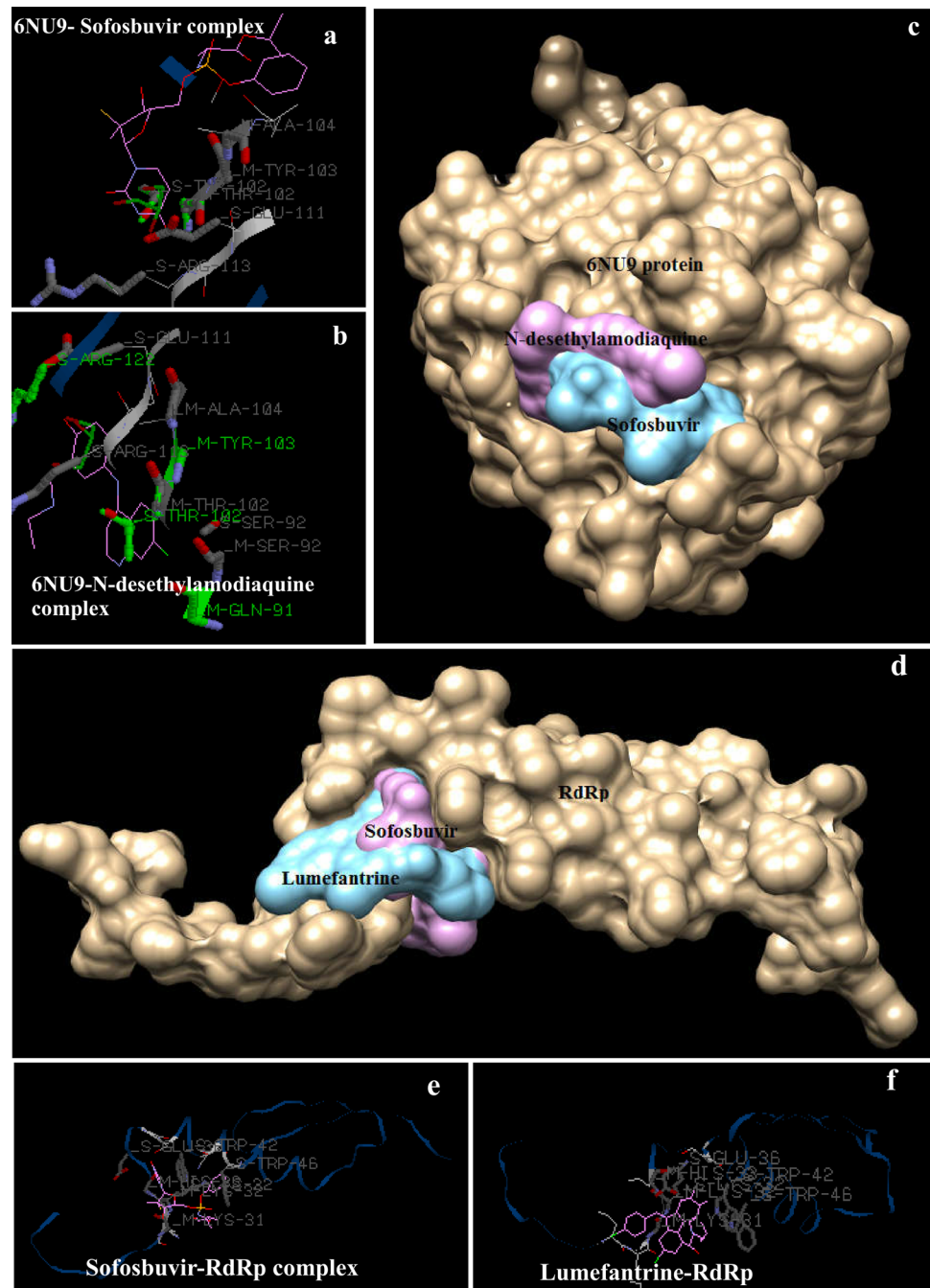
With regard to 6LAT, the selected compounds and their binding scores are presented in Table 2. Pyrimethamine exhibited a higher binding affinity (-97.99 kcal/mol) against the 6LAT target, than Sofosbuvir (- 92.24 kcal/mol), Lumefantrine (- 90.42 kcal/mol), and Amodiaquine (- 90.16 kcal/mol). However, these fitness values were lower than that of Ribavirin (- 99.33 kcal/mol). As shown by Fig. 4a, Pyrimethamine and Ribavirin both interacted

with the M and S domains of the capsid protein. The strong binding of Pyrimethamine is mediated by the H-bonds with 3 amino acids (Ser161, Thr272, Tyr443) and steric interactions with 5 amino acids residues (Pro159, Leu163, Leu164, Asp442, Tyr443 (Table 3) while that of Ribavirin, implicated 9 H-bonds with the following residues Pro142, Thr144, Ser146, Leu155, Asp168, Arg322, Ser324, Thr326, Arg437, and only 4vdW contacts (Thr144, Asp168, Arg322, Arg 437). Both compounds, therefore, showed low similarities in their binding pattern on 6LAT (Fig. 3a). Unlike the two top conformations, Sofosbuvir was found to interact with the M domain only.

Effect on the E2s domain, genotype 1 (3GGQ) and capsid protein of genotype 3 (Z2TN)

On docking with 3GGQ, Lumefantrine showed the most potent binding with the estimated fitness scores of -106.05 kcal/mol greater than that of Sofosbuvir (- 99.81 kcal/mol), and Ribavirin (- 96.99 kcal/mol), followed by Amodiaquine (- 93.64 kcal/mol), Hydroxychloroquine (- 90.55 kcal/mol), Mefloquine (- 88.41 kcal/mol)

Fig. 2 Binding interactions of the best antimalarial drugs docked against the HEV replication targets in comparison with sofosbuvir. **a** hydrophobic interactions of Sofosbuvir with the amino acid residues of the active site of 6NU9; **b** interaction of N-desethylamodiaquine with the active site of 6NU9; **c** 3D conformations of N-desethylamodiaquine (in violet) and Sofosbuvir (in blue) in the binding site of 6NU9; **d** 3D conformations of Lumefantrine (in blue) and Sofosbuvir (in violet) in the binding site of RdRp. **e, f** Hydrophobic amino acid residues interacting in the binding site with Sofosbuvir, and lumefantrine respectively



Pyrimethamine (− 85.06 kcal/mol), Quinine (− 83.61 kcal/mol), Chloroquine (− 81.51 kcal/mol), and Artemisinin (− 71.89 kcal/mol) (Table 2). The strong binding affinity of Lumefantrine was stabilized by 15 amino acid residues including one H-bond with Thr489 and 14 vdW contacts with Gly486, Ser487, Thr489, Gly490, Val492, Gln531, His532, Tyr559, Asn560, Asp567, Gln568, Leu570, Ile581, Ser582 residues (Table 3). However, Sofosbuvir interacted with 13 amino acid residues including 6 H-bonds with Lys544, Asn560, Ser566, Asp567, Gln568, Ser582 and

7 hydrophobic contacts of which 5 were common with Lumefantrine (Tyr559, Asn560, Asp567, Gln568, Ser582), explaining thereby some levels of similarity in the binding mode (Fig. 3b, c).

As far as 2ZTN is concerned, docking results indicated the highest binding scores with Sofosbuvir (− 106.96 kcal/mol), followed by Pyrimethamine (− 105.17 kcal/mol), and N-desethylamodiaquine (− 102.65 kcal/mol), (Table 2). These compounds stabilized the complex through polar and nonpolar interactions. As shown by Table 3, Sofosbuvir is

bound to the M domain of 2ZTN thanks to H-bonds formed with Arg366, Gly367, Gln420, Asp444, Gln446 and hydrophobic interactions with 7 amino acids residues (Arg366, Arg399, Gln420, Gln421, Asp422, Asp444, Gln446). Its binding mode is different from that of the highly interacting antimalarial drugs which exclusively targeted the P domain of this capsid protein (Fig. 3d,e). Pyrimethamine established the H-bonds with 6 amino acids (Gly543, Tyr561, Asn562, Thr563, Thr564, Ser566) and vdW contacts with 11 amino acids residues (Gly543, Lys544, Leu545, Phe 547, Tyr561, Asn562, Thr564, Ser566, Asp567, Thr583, Tyr584) while *N*-desethylamodiaquine only formed H-bonds with 3 amino acid residues (Tyr561, Ser 566, and Asp 567), and steric interactions with 12 amino acid residues including the 11 reported with Pyrimethamine plus Lys554. Therefore, both antimalarial drugs share similarities in their binding modes on 2ZTN.

Pharmacokinetic profiles and side effects of the screened drugs

The analysis of the ADMET properties (Table 4) suggests that the drugs used have good gastrointestinal absorption in general as evidenced by the $F_{30\%}$, and HGI results, and the permeability through the Caco-2 human intestinal cell lines. However, the permeability of these cells to Lumefantrine, Pyrimethamine, Ribavirin, and Sofosbuvir was found lower compared to other drugs. The P-glycoprotein which is a membrane protein, member of the ATP-binding cassette (ABC) transporters superfamily is also known as an important mediator of the efflux of xenobiotics through cells. Several drugs, including Artemisinin, Lumefantrine, Chloroquine, Hydroxychloroquine, Mefloquine, and Quinine showed a high inhibitory potential on this transporter indicating thereby they might interfere with the absorption of other drugs.

Concerning the distribution, Lumefantrine, Chloroquine Hydroxychloroquine were medium. However, Mefloquine Ribavirin and Sofosbuvir presented a good BBB penetration. All the drugs showed a good predicted VD which is comprised in the range of 0.04–20L/kg. Nevertheless, Lumefantrine, Amodiaquine, and Mefloquine displayed high predicted PPB values of 99.91%, 97.33% and 91.86%. Moreover, a good predictive clearance was observed with most of the antimalarial drugs excepted Pyrimethamine, Mefloquine, and Quinine which presented values of 3.89, 2.89, and 1.89 mL/min/kg respectively. All the antimalarial drugs are able to interfere with different CYP isoforms but a high number of interactions was found with Amodiaquine Lumefantrine which is both inhibitor and substrate for 4 distinct CYPs. The examination of the predicted toxicity revealed a high tendency of the antimalarial drugs to induce heart problems and hepatotoxicity excepted Amodiaquine that also

Table 2 Docking scores of antimalarial drugs and anti-hepatitis C drugs on HEV capsid proteins

CryoEM Structure of HEV VLP, genotype 1 (6LAT)				
Amodiaquine	– 90.16	– 76.95	–13.21	0
<i>N</i> -desethylamodiaquine	– 84.35	– 68.02	– 16.32	0
Lumefantrine	– 90.42	– 85.08	– 5.34	0
Chloroquine	– 78.62	– 67.33	– 11.29	0
Mefloquine	– 85.95	– 80.17	– 5.77	0
Hydroxychloroquine	– 82.98	– 70.38	– 12.36	0
Quinine	– 78.51	– 67.9	– 10.62	0
Pyrimethamine	– 97.99	– 80.45	– 17.55	0
Artemisinin	– 74.31	– 58.37	– 15.94	0
Sofosbuvir	– 92.24	– 88.74	– 3.5	0
Ribavirin	– 99.33	– 51.8	– 47.52	0
HEV capsid protein ORF-2, genotype 3 (2ZTN)				
Amodiaquine	– 102.06	– 95.06	– 7	0
<i>N</i> -desethylamodiaquine	– 102.65	– 92.19	– 10.46	0
Lumefantrine	– 89.43	– 83.43	– 6	0
Chloroquine	– 86.49	– 80.57	– 5.92	0
Mefloquine	– 91.46	– 88.96	– 2.5	0
Hydroxychloroquine	– 89.07	– 75.73	– 13.34	0
Quinine	– 98.23	– 91.75	– 6.48	0
Pyrimethamine	– 105.17	– 74.71	– 30.46	0
Artemisinin	– 81.49	– 71.65	– 5.92	0
Sofosbuvir	– 106.96	– 70.94	– 36.02	0
Ribavirin	– 96.04	– 65.73	– 30.31	0
E2s domain, genotype 1 (3GGQ)				
Amodiaquine	– 93.64	– 80.9	– 12.74	0
<i>N</i> -desethylamodiaquine	– 84.32	– 70.45	– 13.87	0
Lumefantrine	– 106.05	– 95.44	– 10.61	0
Chloroquine	– 81.51	– 78.01	– 3.5	0
Mefloquine	– 88.41	– 78.07	– 10.34	0
Hydroxychloroquine	– 90.55	– 75.16	– 15.39	0
Quinine	– 83.61	– 75.21	– 8.4	0
Pyrimethamine	– 85.06	– 55.04	– 30.02	0
Artemisinin	– 71.89	– 64.23	– 7.67	0
Sofosbuvir	– 99.81	– 78.67	– 21.14	0
Ribavirin	– 96.99	– 57.87	– 39.11	0

Bold values indicate compounds with the highest binding energies

demonstrated a low carcinogenic potential. However, as with other drugs, the potential side effects of these compounds on the respiratory systems is to fear.

In vitro effects of lumefantrine, amodiaquine and *N*-desethylamodiaquine on gt 3 HEV replicon cells

In order to validate the computational predictions, the activity of anti-malarial compounds (Lumefantrine, Amodiaquine and *N*-desethylamodiaquine) was tested on the efficiency of replication of the HEV p6GLuc replicon in PLC3 cells

Table 3 Receptor-ligand interactions of the top docking drugs with the different HEV targets

Target	Sofosbuvir	Ribavirin	Amodiaquine	N-desethyl amodiaquine	Pyrimeth-amine	Lumefantrine
6NU9	H-bond VdW	Ser92, Thr102, Ala105, Arg113 Gln91, Ser92, Thr102, Tyr103, Ala104, Ala105, Glu111, Val112, Arg113, Arg122		Gln91, Thr 102, Tyr103, Arg122 Gln91, Ser92, Thr102, Tyr103, Ala104, Glu111, Arg113, Arg122		Gln91, Ser92, Thr102, Tyr103, Ala104, Glu111, Val112, Arg113, Arg122
6LAT	H-bond	Ser403 Pro142, Thr144, Ser146, Leu155, Asp168, Arg322, Ser324, Thr326, Arg437			Ser161, Thr272, Tyr443	Asn560
	VdW	Met350, Lys351, Phe355, Val402, Ser403, Ala404, Gly406, Glu407, Pro408	Thr144, Asp168, Arg322, Arg 437			Gln531, Tyr532, Tyr559, Ala565, Ser566, Asp567, Gln568, Ser582
2ZTN	H-bond	Arg366, Gly367, Gln420, Asp444, Gln446		Tyr561, Ser566, Asp567	Gly543, Tyr561, Asn562, Thr563, Thr564, Ser566	
	VdW	Arg366, Arg399, Gln420, Gln421, Asp422, Asp444, Gln446		Gly543, Lys544, Leu545, Phe547, Lys554, Tyr561, Asn562, Thr564, Ser566, Ser566, Asp567, Thr583, Tyr584		
3GGQ	H-bond	Lys544, Asn560, Ser566, Asp567, Gln568, Ser582				Thr489
	VdW	Tyr559, Asn560, Ala565, Ser566, Asp567, Gln568, Ser582				Gly486, Ser487, Thr489, Gly490, Val492, Gln531, His532, Tyr559, Asn560, Asp567, Gln568, Leu570, Ile581, Ser582
RdRp	H-bond	Lys31, Trp42, Trp46	Lys32			
	VdW	Trp30, Lys31, Lys32, His33, Glu 36, Gly 38, Trp42, Asn43, Trp46	Trp30, Lys31, Lys32, His33, Glu 36, Gly 38, Trp42, Asn43, Trp46			Phe29, Trp30, Lys31, Lys32, His33, Glu 36, Gly 38, Trp42, Asn43, Trp46

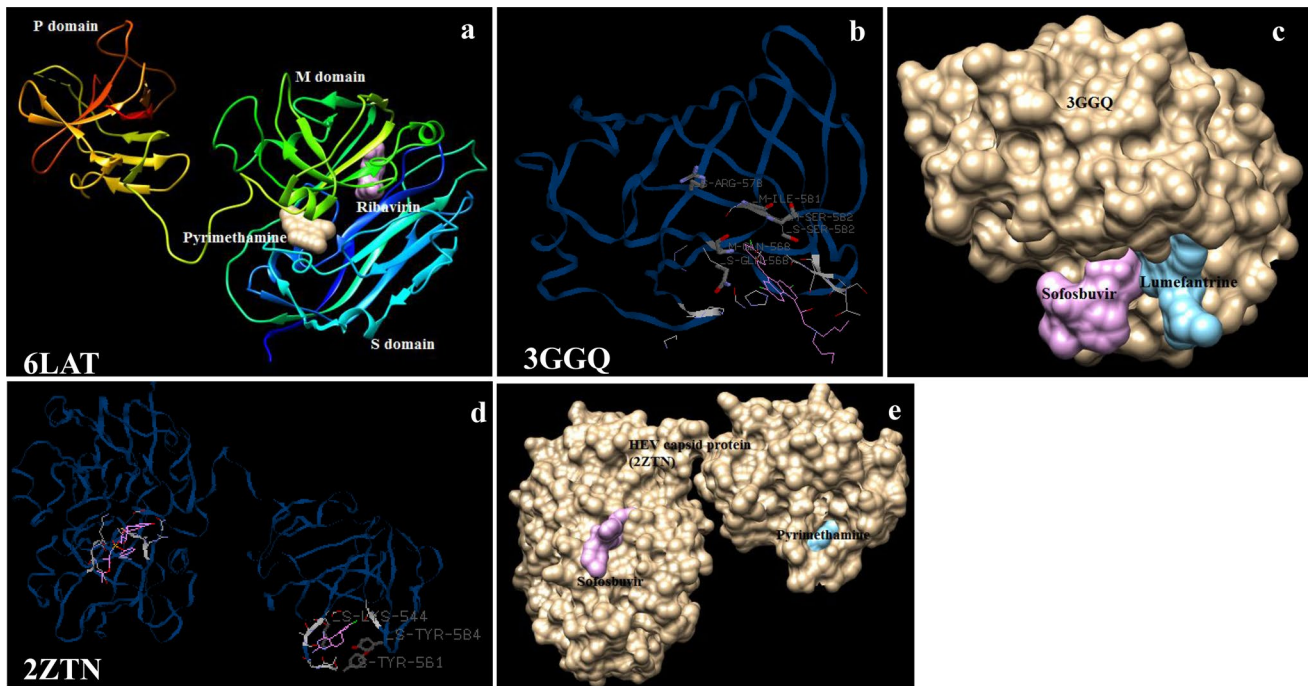


Fig. 3 Binding interactions of the best antimalarial drugs docked against the HEV capsid proteins in comparison with Sofosbuvir and Ribavirin. **a** Interactions of Pyrimethamine and Ribavirin with the conserved domains of the 6LAT target; **b** 2D conformations of Lumefantrine with the E2s domain (3GGQ) showing hydrophobic interactions with Gly486, Ser487, Thr489, Gly490, Val492, Gln531, His532, Tyr559, Asn560, Asp567, Gln568, Leu570, Ile581, Ser582; **c** 3D conformations of Lumefantrine (in blue) and Sofosbuvir (in violet) in the 3GGQ target. **d**, **e** 2D and 3D conformations of Lumefantrine and Sofosbuvir in 2ZTN

conformations of Lumefantrine (in blue) and Sofosbuvir (in violet) in the 3GGQ target. **b** 2D conformations of Lumefantrine with the E2s domain (3GGQ) showing hydrophobic contacts with Gly486, Ser487, Thr489, Gly490, Val492, Gln531, His532, Tyr559, Asn560, Asp567, Gln568, Leu570, Ile581, Ser582; **c** 3D conformations of Lumefantrine (in blue) and Sofosbuvir (in violet) in the 3GGQ target. **d**, **e** 2D and 3D conformations of Lumefantrine and Sofosbuvir in 2ZTN

during the course of 5 days post-electroporation. The replication kinetics of the HEV p6GLuc replicon in the presence of these compounds were compared to the kinetics of (i) the untreated HEV p6GLuc as positive control, (ii) the HEV p6GLuc treated with Sofosbuvir as a known HEV inhibitor (Dao Thi et al. 2016) and (iii) the HEV p6GLuc GAD mutant as replicative-deficient negative control. Surprisingly, Lumefantrine does not seem to impact p6GLuc replication efficiency at the concentrations used (10, 5 and 1 μM) (Fig. 4a). Indeed, in the presence of 10 μM of Lumefantrine, the p6GLuc replication efficiency is comparable to the replication fold of the untreated p6GLuc (Fig. 5b). In addition, PLC3 viability was not affected at concentrations of 1, 5 and 10 μM of Lumefantrine (Fig. 5b). On the contrary, Amodiaquine drastically decreased cell viability by 49% ($P < 0.001$) and 85% ($P < 0.001$) at 5 and 10 μM concentrations, respectively (Figs. 4b and 5a). While the replication efficiency of PLC3 cells in the presence of these concentrations of Amodiaquine drops closer to that of sofosbuvir-treated replicons, Amodiaquine at 1 μM appears as the most efficient concentration. Indeed, the decrease of viral replication at this concentration is not accompanied by any cytotoxicity (Figs. 5a and 5b). Moreover, the N-desethylamodiaquine compound, which is the major biologically active metabolite

of Amodiaquine (Zhang et al. 2017), distinctly lowered the replication efficiency of the p6GLuc replicon at a concentration of 1 μM as compared to the untreated replicon. Interestingly, at this concentration, a significant decrease ($P < 0.05$) in replication fold of the HEV p6GLuc replicon was recorded, almost reaching 50% inhibition in comparison to the untreated p6GLuc replication efficiency (Fig. 5a) and the PLC3 cells displayed close to 91% of viability (Fig. 5b). However, N-desethyl Amodiaquine was cytotoxic to PLC3 cells at concentrations of 5 and 10 μM (Fig. 5b).

Discussion

Hepatitis E is an emerging viral disease in developing countries including Cameroon where human and zoonotic transmissions have been signaled (Amougou et al. 2017; Modiyinji et al. 2018, 2019; Wilson et al. 2020). In spite of recent progress in the antiviral drug development, therapeutic options against HEV are still limited. Drug repurposing has been proposed recently as an innovative approach to rapidly identify efficient drugs against viral diseases without the need to undergo multiple clinical trials (Kinast et al. 2019). In this study, we investigated the in silico potential

Table 4 Functions and ADMET properties of the different drugs

Drugs	AMQ	ART	LUM	CHL	OH-CHL	MFQ	PYR	QUI	RBV	SOF
Functions	Antimalarial drugs									
A	Caco-2 permeability	Good - 4.964	Low - 5.34	Good - 4.62	Good - 4.59	Good - 5.11	Low - 5.47	Good - 4.78	Low - 5.65	Low - 6.08
	MDCK permeability (cm/s)	Medium 1.4×10^{-5}	High 6×10^{-5}	Medium 1.1×10^{-5}	Medium 1.1×10^{-5}	Medium 1.2×10^{-5}	High 3.9×10^{-5}	Medium 1.7×10^{-5}	Medium 1.1×10^{-5}	Medium 1.1×10^{-5}
	P-gp inhibitor	Poor	High	High	High	High	Poor	High	Poor	Poor
	P-gp substrate	Poor	High	High	High	Poor	High	High	Medium	Poor
	F _{30%}	Good	Good	Good	Good	Good	Good	Good	Medium	Good
	HGI	Good	Good	Good	Good	Good	Good	Good	Good	Good
D	BBB penetration	Medium	Poor	Poor	Poor	Good	Medium	Poor	Good	Good
	PPB (%)	97.33	99.91	84.03	69.60	91.86	88.83%	83.78	15.12	37.207
	VD (L/kg)	2.4	2.99	3.2	2.25	5.34	0.79	2.32	0.6	1.09
M	CYP inhibitors	1A2,2C19,2D6,	1A2, 2C19, 2D6	1A2, 2D6	1A2, 2D6	1A2, 2D6	1A2	2D6	-	-
	CYP substrates	1A2, 2D6	1A2, 3A4	1A2, 2D6	1A2, 2D6	2C19, 2D6	1A2	1A2, 2D6, 2C19	-	2C9
E	Clearance (mL/min/kg)	Good	Good	Good 6.16	Good	Poor	Poor	Poor	Poor	Good
	T _{1/2}	7.5	7.57	Short	6.43	2.82	3.89	1.89	4.2	6.43
Predicted Toxicity	hERG blockers	Medium	Short	Short	Short	Short	High	Short	High	High
	H-HT	Poor	High	High	High	High	High	Medium	Poor	Poor
	Carcinogenicity	Medium	High	High	High	High	High	High	Medium	High
	Respiratory Toxicity	Low	Low	Low	Low	Low	High	Medium	Poor	Poor
		High	Medium	High	High	High	High	High	Poor	Medium

A Absorption, M Metabolism, AMQ amodiaquine, ART artemisinin, D Distribution, E: Excretion LUM lumefantrine, CHL chloroquine, OH-CHL, hydroxychloroquin, MFQ mefloquine, PYR pyrimethamine, QUI quinine, RBV ribavirin, SOF sofosbuvir

Compounds with a good predicted PPB value (< 90%) are considered as normally distributed. However, those with high PPB values (>90%) are shown in Bold and are considered as poorly distributed

of 8 licensed antimalarial drugs against HEV, and compared it with two approved anti-hepatitis C drugs (Sofosbuvir and ribavirin) which experimentally demonstrated in vitro effects against HEV (Thi et al. 2016). Moreover, the biological effects of the best docked drugs were evaluated experimentally using gt 3 HEV replicon systems.

Concerning the computational screening against the Zinc-binding non-structural protein (6NU9), Sofosbuvir, *N*-desethylamodiaquine, and Amodiaquine demonstrated the most potent affinities with fitness scores of -98.22, -93.5, and, - 89.9 kcal/mol respectively compared to Ribavirin (Table 1). The high score of *N*-desethylamodiaquine relative to other drugs may be explained by similarities between the binding mode of this metabolite and that of Sofosbuvir. Indeed, both compounds form H-bonds with Thr 102 (Table 3) and show hydrophobic interactions with almost the same amino acid residues. First studies on the biophysical and structural characterization of 6NU9 suggested that this protein might correspond to HEV protease (Proudfoot et al. 2019). Therefore, our data indicate that these drugs could inhibit viral replication by highly interfering with the HEV protease. In order to check whether the affinities of these drugs could be also high on other targets of viral replication, their effects were virtually screened against the RdRp. Greater binding scores were found with Lumefantrine, and Amodiaquine compared to Ribavirin, but their affinities for this target were still lower than that of Sofosbuvir (Table 1). Moreover, the top docked conformations were stabilized by the same hydrophobic contacts (Table 3),

indicating therefore that both antimalarial drugs could also highly target the RdRp better than ribavirin with a binding mode similar to Sofosbuvir.

In order to validate these in silico predictions about the anti-replicative potential of these two drugs, their effects were evaluated in vitro on PLC3 cell lines using a replicon construct (HEV gt 3 p6GLuc replicon). Our results showed Lumefantrine was not active at the tested concentrations (1–10 μ M), contrary to *N*-desethylamodiaquine, a major metabolite from Amodiaquine which significantly ($P < 0.001$) decreased viral replication without affecting the cell viability when tested at 1 μ M concentration (Fig. 5a, b). The here-generated data suggest a positive correlation between the in silico effect of *N*-desethylamodiaquine on HEV protease and the antiviral effect observed in cell culture, considering the highest binding energy score obtained (- 93.5 kcal/mol) on 6NU9, relative to other antimalarial drugs and the significant viral inhibition achieved with this compound at 1 μ M concentration in p6GLuc replicon. Likewise, a strong positive correlation has been observed between the great binding scores of Sofosbuvir on replication targets and the experimental data. *N*-desethylamodiaquine could be therefore regarded as an inhibitor of the viral replication with similar effects to Sofosbuvir and that strongly and preferentially targets the HEV protease with little affinity on RdRp. Moreover, a moderate affinity was recorded between this compound and the HEV entry targets (Table 2). These results are in line with subsequent studies which demonstrated that Amodiaquine was able to inhibit

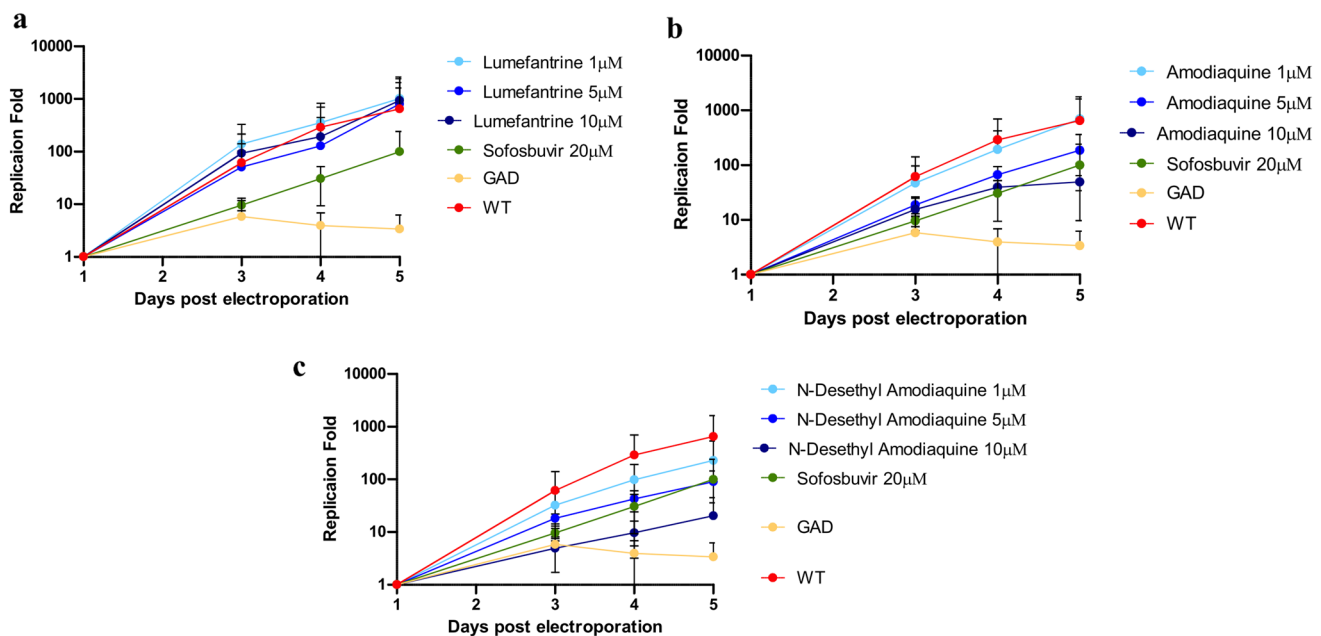
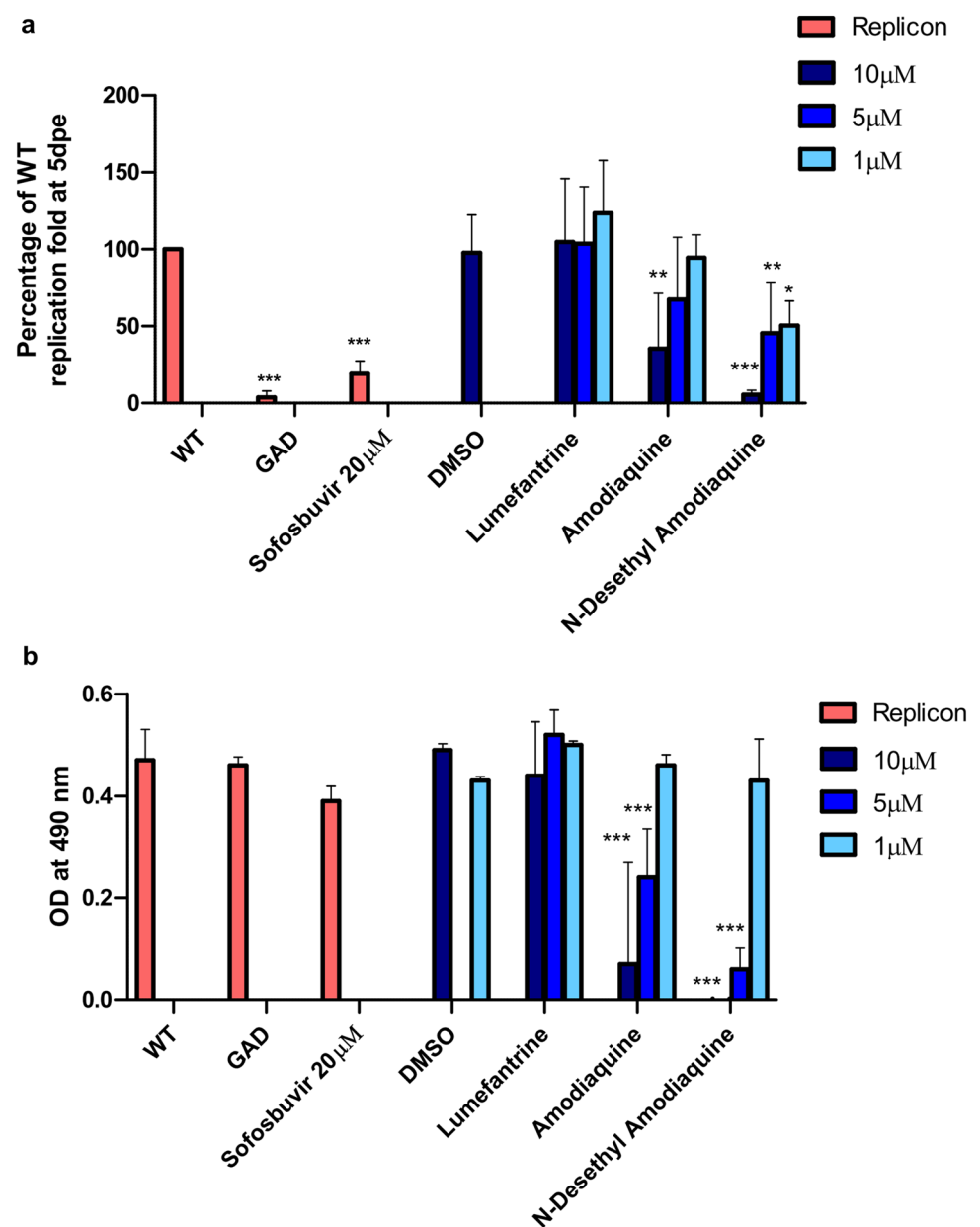


Fig. 4 Replication efficiency of the HEV p6GLuc replicon in the presence of Lumefantrine (a), Amodiaquine (b) and *N*-desethylamodiaquine (c) at the concentrations of 1, 5 and 10 μ M. The p6GLuc

GAD mutant and the p6GLuc inhibited by Sofosbuvir (20 μ M) served as negative controls. The replication folds were normalized to 1dpe. $N = 3$

Fig. 5 Replication efficiencies (a) and level of cell viability (b) in PLC3 replicon cells treated with the compounds Sofosbuvir (20 μ M), Lumefantrine, Amodiaquine, and *N*-desethylamodiaquine at 5dpe. The replication efficiencies were plotted as percentages of the untreated p6Gluc replication fold. $N=3$. Viability cell was depicted as intensity of the optic density (OD) at 490 nm



the replication of dengue virus type 2 (Boonyasuppayakorn et al. 2014) and Zika virus (Han et al. 2018). Nevertheless, complementary studies are required to better understand the mechanism of action of this antimalarial drug. We also found that Lumefantrine is negatively correlated to viral inhibition as the lack of activity on cell models contrasts with the high binding scores obtained on the viral targets, especially on RdRp. These results are also similar to that of Barger-Kamate et al. who found a moderate efficacy of the Lumefantrine-artemether association against the cytomegalovirus 25 in a clinical study in Malian patients (Barger-Kamate et al. 2016). The lack of effect of Lumefantrine in this study might be due either to the low concentrations used or to the genotype and the replicon used. Indeed, the mutations

inserted in the sequence of this replicon would affect the binding and therefore the susceptibility to the antimalarial drug as demonstrated in previous studies with HCV-resistant mutants (Nitta et al. 2016). Furthermore, pharmacokinetic considerations are not to be excluded. Biocomputational analysis of the ADMET profile of Lumefantrine revealed a low permeability through biological membranes, and a higher protein-bound predictive value compared to Amodiaquine. These factors might be indicative of a poor therapeutic index as earlier reported (Dong et al. 2018). In fact, previous studies demonstrated that the binding of a drug to proteins in plasma may negatively influence its pharmacodynamic behavior, as it decreases the concentration of the free drug to the target site (Dong et al. 2018; Smith and Waters

2019). In addition, both compounds also interact with almost the same CYP isoforms but Lumefantrine seems to be a specific CYP 3A2 substrate while Amodiaquine is particularly metabolized by CYP2D6. This difference might explain the rapid inactivation of Lumefantrine and therefore the short half-time observed.

HEV capsid is an important element in viral pathogenesis as it is involved in host-virus interactions, viral assembly, and immunogenicity (Liu et al. 2011). Thanks to techniques like X-crystallography and CryoEM, the capsid protein has been extensively studied and characterized into 3 structural domains including the shell domain (S domain, aa 118–317), a middle domain (M domain, aa 318–451), and a protrusion domain or E2s domain (P domain, aa 452–606) on HEV virus-like particles (HEV VLPs) purified from robust cell culture systems (Bai et al. 2020). Structure alignment with these domains revealed that M and S were highly conserved whereas the P domain was extremely variable (Zhang et al. 2018). The 6LAT protein, presented here, is an asymmetric unit of the capsid protein obtained from HEV gt1 particles. Docking results showed high binding affinities of this protein with Ribavirin and Pyrimethamine on the conserved domains which are tightly associated (Fig. 3a). Ribavirin was found to strongly collide with the M and S domains through 9 H-bonds with Pro142, Thr144, Ser146, Leu155, Asp168, Arg322, Ser324, Thr326, Arg437, and 4 vdW contacts (Thr144, Asp168, Arg322, Arg 437) while Pyrimethamine formed H-bonds with 3 amino acids (Ser161, Thr272, Tyr443) and steric interactions with 5 amino acid residues (Pro159, Leu163, Leu164, Asp442, Tyr443 (Table 3). Studies on the functions of these domains showed that the S domain builds the integral shell of the HEV particle, with a cluster of basic amino acid residues that contribute to neutralizing negative charges of the HEV genomic RNA (Guo et al. 2009). Other studies indicated that the M domain also partially participated in this function but its interaction with the P domain makes it essential in cell-attachment. In a previous study reported by Schofield et al., (Schofield et al. 2003), it has been shown that neutralizing antibodies interfered with HEV entry steps by recognizing linear epitopes located in the M domain of capsid protein. Similar findings were also reported by another group (He et al. 2008), confirming thereby the possibility for Pyrimethamine to inhibit cell-attachment of gt 1 particles.

In order to confirm this antiviral potential on other genotypes, especially on zoonotic strains, antimalarial drugs were screened against the ORF-2 protein, of gt3 (2ZTN). Similarly, Sofosbuvir and Pyrimethamine stood out as highly interacting compounds. However, their binding patterns were strikingly different. The affinity of Sofosbuvir was still located on the conserved domains through interactions with 12 amino acid residues whereas that of Pyrimethamine was more oriented on the E2s domain via interactions

with 17 amino acid residues including 6 in H-bond and 11 in steric interactions. Most of the amino acids involved in hydrophobic interactions with Pyrimethamine was similar to that of Amodiaquine. The great difference especially originated from H-bonds formed by Pyrimethamine with Gly543, Tyr561, Asn562, Thr563, Thr564, Ser566. These results prove that the affinity of Pyrimethamine for the HEV capsid protein changes according to mutations due to the genotypes. Besides, it also pointed out the ability of this compound to act against human and zoonotic HEV strains. Several studies previously demonstrated the capacity of neutralizing antibodies including 8C11 and 8G12, to bind on E2s domain (Guo et al. 2015; Tang et al. 2011; Zheng et al. 2019). It has been suggested that the loop region formed by amino acid residues 550–566 and 580–593 of this domain, contained hypervariable amino acids which help the viral particle to escape the antibody recognition (Liu et al. 2011). Therefore, interferences with amino acids found in this region might allow decreasing the immunogenicity of the HEV particle and its infectivity as well, as, these sugar-binding sites were also found to be implicated in cell-attachment (Guo et al. 2015). In this study, Pyrimethamine showed hydrophobic (Tyr561, Asn562, Thr564, Ser566, Asp567, Thr583, Tyr584) and hydrogen (Tyr561, Asn562, Thr563, Thr564, Ser566) interactions in E2s loops of HEV gt3, indicating it may decrease the immunogenicity of these gt 3 particles and their binding to the host cell.

The importance of dimerization of the E2s domain as a prerequisite for HEV infectivity has been previously documented (Guo et al. 2015; Liu et al. 2011; Tang et al. 2011; Zhang et al. 2018). As the E2s region, seemed to be a preferred target for Pyrimethamine on gt3 viral particles, all antimalarial compounds were specifically docked against this domain using a gt1 viral strain. As shown by Table 2, surprisingly, Lumefantrine was the antimalarial compound with the greatest binding score (– 106.05 kcal/mol) followed by Sofosbuvir, and Ribavirin (– 99.81 and – 96.81 kcal/mol respectively). However, Pyrimethamine only showed a low fitness score (– 85.06 kcal/mol). The genetic diversity of viral strains has certainly negatively affected the Pyrimethamine binding site on 3GGQ. In a previous study, Zheng et al. reported the monoclonal antibodies could bind into the E2s domain in two manners: either directly on the epitope located on the top of the protrusion domain as found with 3B6 antibody or on the flanking side as shown by 8C11 antibodies (Zheng et al. 2019). The interaction with the epitope on the top inhibited viral attachment while preserving viral integrity whereas interaction with the flanking region directly disorganized the icosahedral arrangement of capsids and split the viral particles into small pieces. In an attempt to characterize the amino acids involved in the 8C11 binding site using gts 1 and 4 HEV capsids, authors found that 8C11 was specific to gt 1 and that 8C11 epitope

regions contained Ser497 and Ala575, for gt 1 whereas gt 4 possessed Thr497 and Pro575. Ser 497 was found in H-bond with 8C11 (gt1) while Arg 512 is crucial in gt4 interactions (Tang et al. 2011). Our results tend to show that Lumefantrine is more specific to E2s domain of gt 1 while Pyrimethamine is specific on gt 3. Moreover, Sofosbuvir, and Lumefantrine share similarity in their binding patterns on the E2s region of gt1 particles as they mainly interact with the same amino acid residues in antibody-binding region. Further investigations should be conducted to clarify whether this interaction directly destroys the structure of HEV capsid or impede viral attachment.

Conclusion

In conclusion, among all docked antimalarial drugs, Amodiaquine, Lumefantrine, and Pyrimethamine stood out as promising candidates for repurposing against HEV. Whether Amodiaquine is advantaged by the N-desethylamodiaquine, its main human metabolite, which is highly active on HEV replicon systems in vitro and exhibits a strong binding score and specificity for the Zn-binding nonstructural protein, Lumefantrine, however, seems to be handicapped by pharmacokinetics constraints which limits its biological effect although having great binding scores with the RdRp and E2s domain. In fact, the ADMET profile of both drugs revealed a low permeability of Lumefantrine and an affinity for the CYP3A2 which could rapidly metabolize the drug and therefore inactive it, justifying thereby the lack of activity on replicon systems. Unlike these drugs, Pyrimethamine seemed to collide better on HEV entry through interference with the capsid protein. Further in vivo and in vitro experiments are necessary to validate the anti-HEV potential of these antimalarial drugs and elucidate the mechanism of action.

Supplementary Information The online version contains supplementary material available at <https://doi.org/10.1007/s40203-021-00093-y>.

Acknowledgements We are thankful to Dr. Karin Seron from the Institute Pasteur of Lille for the critical review of this manuscript. This research received no specific grant from any funding agency in the public, commercial, or not-for-profit sectors.

Funding No funding has been received to conduct this study.

Declarations

Conflict of interest The authors have no conflict of interest to disclose for this manuscript.

Ethical Approval This manuscript does not include any human participants or animals.

Availability of Data and Material The data used in this study will be made available upon reasonable request from the corresponding author.

References


- Amougou AM, Atangana PJA, Noah Noah D, Moundipa PF, Pineau P, Njoum R (2007) Hepatitis E virus infection as a promoting factor for hepatocellular carcinoma in Cameroon: preliminary Observations. *Int J Infect Dis* [Internet] Elsevier BV 64:4–8 Available at <https://pubmed.ncbi.nlm.nih.gov/28847760/> [cited 2020 Oct 12]
- Aslam SM (2017) Case study an interesting case of complicated falciparum malaria and hepatitis E virus co-infection. *Int J Clin Cases Investig* 6(3):35–37
- Bai C, Cai J, Han P, Qi J, Yuen KY, Wang Q (2020) The crystal structure of the emerging human-infecting hepatitis E virus E2s protein. *Biochem Biophys Res Commun* [Internet]. Elsevier Ltd 532(1):25–31 <https://doi.org/10.1016/j.bbrc.2020.07.074>
- Barger-Kamate B, Forman M, Sangare CO, Haidara ASA, Maiga H, Vaidya D, et al (2016) Effect of artemether-lumefantrine (Coartem) on cytomegalovirus urine viral load during and following treatment for malaria in children. *J Clin Virol* [Internet]. Elsevier BV 77:40–5 Available at: <https://www.ncbi.nlm.nih.gov/pmc/articles/PMC4792724/> [cited 2020 Oct 20]
- Boonyasuppayakorn S, Reichert ED, Manzano M, Nagarajan K, Padmanabhan R (2014) Amodiaquine, an antimalarial drug, inhibits dengue virus type 2 replication and infectivity. *Antiviral Res Elsevier* 106(1):125–134. Available at <https://www.ncbi.nlm.nih.gov/pmc/articles/PMC4523242/> [cited 2020 Oct 15]
- Dao Thi VL, Debing Y, Wu X, Rice CM, Neyts J, Moradpour D, et al (2016) Sofosbuvir inhibits hepatitis e virus replication in vitro and results in an additive effect when combined with ribavirin. *Gastroenterology* 150(1):82–85.e4. <https://doi.org/10.1053/j.gastro.2015.09.011>
- Doceul V, Bagdassarian E, Demange A, Pavo N (2016) Zoonotic HEP-ATITIS E virus: classification, animal reservoirs and transmission routes. *Viruses* 8(10):1–24
- Dong J, Wang N-N, Yao Z-J, Zhang L, Cheng Y, Ouyang D, et al (2018) ADMETlab: a platform for systematic ADMET evaluation based on a comprehensively collected ADMET database. *J Cheminform* 10(1):29. Available at: <https://jcheminf.biomedcentral.com/articles/10.1186/s13321-018-0283-x> [cited 2021 Mar 29]
- Donnelly MC, Scobie L, Crossan CL, Dalton H, Hayes PC, Simpson KJ (2017) Review article: hepatitis E—a concise review of virology, epidemiology, clinical presentation and therapy. *Aliment Pharmacol Ther* 46(2):126–141
- Emerson SU, Nguyen HT, Torian U, Mather K, Firth AE. An essential RNA element resides in a central region of hepatitis E virus ORF2. *J Gen Virol* 94(PART7):1468–76. Available at <https://www.ncbi.nlm.nih.gov/pmc/articles/PMC3709636/> [cited 2021 Mar 28]
- Fraga M, Gouttenoire J, Sahli R, Chtioui H, Marcu C, Pascual M, et al (2019) Sofosbuvir add-on to ribavirin for chronic hepatitis e in a cirrhotic liver transplant recipient: a case report. *BMC Gastroenterol* 19(1):76. Available at <https://bmcgastroenterol.biomedcentral.com/articles/10.1186/s12876-019-0995-z> [cited 2020 Oct 13];
- Gouttenoire J, Pollán A, Abrami L, Oechslein N, Mauron J, Matter M, et al. Palmitoylation mediates membrane association of hepatitis E virus ORF3 protein and is required for infectious particle secretion. *PLoS Pathog* 14(12). Available at <https://pubmed.ncbi.nlm.nih.gov/30532200/> [cited 2020 Oct 23]
- Gu Y, Tang X, Zhang X, Song C, Zheng M, Wang K, et al. Structural basis for the neutralization of hepatitis E virus by a cross-genotype

- antibody. *Cell Res Nature Publishing Group* 25(5):604–620. Available at <https://www.nature.com/articles/cr201534> [cited 2020 Oct 16]
- Guex N, Peitsch MC, Schwede T (2009) Automated comparative protein structure modeling with SWISS-MODEL and Swiss-Pdb-Viewer: a historical perspective. *Electrophoresis* 30:S162–S173
- Guu T, Liu Z, Ye Q, Mata D, Li K, Yin C et al (2009) Structure of the hepatitis E virus-like particle suggests mechanisms for virus assembly and receptor binding. *Proc Natl Acad Sci USA* 106:12992–12997
- Han Y, Mespèrès T, Xu H, Quan Y, Wainberg MA. The antimalarial drug amodiaquine possesses anti-ZIKA virus activities. *J Med Virol John Wiley and Sons Inc* 90(5):796–802. Available at: <https://onlinelibrary.wiley.com/doi/abs/10.1002/jmv.25031> [cited 2020 Oct 15]
- He S, Miao J, Zheng Z, Wu T, Xie M, Tang M, et al. Putative receptor-binding sites of hepatitis E virus. *J Gen Virol Microbiology Soc* 89(1):245–249. Available at: <https://www.microbiologyresearch.org/content/journal/jgv/10.1099/vir.0.83308-0> [cited 2020 Oct 16]
- Kenney SP, Meng XJ (2019) Hepatitis E virus genome structure and replication strategy. *Cold Spring Harb Perspect Med* 9(1):1–18
- Kinast V, Burkard TL, Todt D, Steinmann E (2019) Hepatitis E virus drug development. *Viruses* 11(6):1–16
- Liu Z, Jane Y, Zhang J (2011) Structure and function of the hepatitis E virus capsid related to hepatitis E pathogenesis. In: Mukomolov DS, editor. *Viral Hepat—Sel. Issues Pathog. Diagnostics [Internet]*. In Tech; 2011. p. 141–152. Available at <http://www.intechopen.com/books/viral-hepatitis-selected-issues-of-pathogenesis-is-and-diagnostics/structure-and-function-of-the-hepatitis-e-virus-capsid-related-to-hepatitis-e-pathogenesis>
- Lozano R, Naghavi M, Foreman K, Lim S, Shibuya K, Aboyans V, et al. Global and regional mortality from 235 causes of death for 20 age groups in 1990 and 2010: a systematic analysis for the Global Burden of Disease Study 2010. *Lancet Lancet Publishing Group* 380(9859):2095–128. Available at: <https://pubmed.ncbi.nlm.nih.gov/23245604/> [cited 2020 Oct 12]
- Mirdita M, von den Driesch L, Galiez C, Martin MJ, Söding J, Steinegger M (2016) Uniclust databases of clustered and deeply annotated protein sequences and alignments. *Nucleic Acids Res* 45:D170–D176
- Modiyinji AF, Atsama MA, Monamele GC, Nola M, Njouom R. High seroprevalence of hepatitis e among pigs suggests an animal reservoir in Cameroon. *J Infect Dev Ctries [Internet]* 12(8):676–679. Available at <https://jicd.org/index.php/journal/article/view/10310> [cited 2020 Oct 13]
- Modiyinji AF, Amougou-Atsama M, Monamele CG, Nola M, Njouom R (2019) Seroprevalence of hepatitis E virus antibodies in different human populations of Cameroon. *J Med Virol John Wiley and Sons Inc.* 91(11):1989–94. Available at: <https://pubmed.ncbi.nlm.nih.gov/31297845/> [cited 2020 Oct 12]
- Modiyinji AF, Rivero-Juarez A, Lopez-Lopez P, Atsama MA, Monamele CG, Nola M, et al (2020) First molecular characterization of the hepatitis E virus in humans in Cameroon: confirmation of the HEV outbreak in Touboro, North-Cameroon. *J Med Virol.* Available at: <https://pubmed.ncbi.nlm.nih.gov/32639604/> [cited 2020 Oct 12]
- Montpellier C, Wychowski C, Sayed IM, Meunier JC, Saliou JM, Ankavay M, et al (2018) Hepatitis E virus lifecycle and identification of 3 forms of the ORF2 capsid protein. *Gastroenterology [Internet] WB Saunders* 154(1):211–223.e8. Available at: <http://www.gastrojournal.org/article/S0016508517361796/fulltext> [cited 2021 Mar 28]
- Nair VP, Anang S, Subramani C, Madhvi A, Bakshi K, Srivastava A, et al (2016) Endoplasmic reticulum stress induced synthesis of a novel viral factor mediates efficient replication of genotype-1 hepatitis E virus. *PLoS Pathog [Internet] Public Library of Science* 12(4). Available at <https://pubmed.ncbi.nlm.nih.gov/27035822/> [cited 2020 Oct 13]
- Nan Y, Wu C, Zhao Q, Sun Y, Zhang YJ, Zhou EM (2018) Vaccine development against zoonotic hepatitis E virus: open questions and remaining challenges [Internet]. *Front Microbiol Front Media SA.* Available at: <https://www.ncbi.nlm.nih.gov/pmc/articles/PMC5827553/> [cited 2020 Oct 23]
- Navaneethan U, Al Mohajer M, Shata MT (2018) Hepatitis E and pregnancy: Understanding the pathogenesis [Internet]. *Liver Int NIH Public Access* : 1190–1199. Available at: <https://www.ncbi.nlm.nih.gov/pmc/articles/PMC2575020/> [cited 2020 Oct 12].
- Nimgaonkar I, Ding Q, Schwartz RE, Ploss A (2018) Hepatitis E virus: advances and challenges. *Nat Rev Gastroenterol Hepatol [Internet] Nature Publishing Group* 15(2):96–110. Available at <http://www.nature.com/articles/nrgastro.2017.150> [cited 2020 Oct 23]
- Nitta S, Asahina Y, Matsuda M, Yamada N, Sugiyama R, Masaki T, et al. Effects of resistance-associated NS5A mutations in hepatitis C virus on viral production and susceptibility to antiviral reagents. *Sci Rep [Internet] Nature Publishing Group* 6(1):1–9. Available at: www.nature.com/scientificreports [cited 2021 Mar 28]
- Passini E, Britton OJ, Lu HR, Rohrbacher J, Hermans AN, Gallacher DJ, et al. Human in silico drug trials demonstrate higher accuracy than animal models in predicting clinical pro-arrhythmic cardiotoxicity. *Front Physiol* 8(SEP):1–15.
- Proudfoot A, Hyrina A, Holdorf M, Frank AO, Bussiere D (2019) First crystal structure of a nonstructural hepatitis e viral protein identifies a putative novel zinc-binding protein. *J Virol American Society for Microbiology* 93(13). Available at: <https://pubmed.ncbi.nlm.nih.gov/31019049/> [cited 2020 Oct 14]
- Rein DB, Stevens GA, Theaker J, Wittenborn JS, Wiersma ST (2012) The global burden of hepatitis E virus genotypes 1 and 2 in 2005. *Hepatology [Internet]* 55(4):988–97. Available at: <https://pubmed.ncbi.nlm.nih.gov/22121109/> [cited 2020 Oct 12]
- Sachdeva C, Wadhwa A, Kumari A, Hussain F, Jha P, Kaushik NK (2020) In silico potential of approved antimalarial drugs for repurposing against COVID-19. *Omi A J Integr Biol* 24(10):568–581
- Schofield DJ, Purcell RH, Nguyen HT, Emerson SU (2003) Monoclonal antibodies that neutralize HEV recognize an antigenic site at the carboxyterminus of an ORF2 protein vaccine. *Vaccine* 22(2):257–267
- Shukla J, Saxena D, Rathinam S, Lalitha P, Joseph CR, Sharma S, et al (2012) Molecular detection and characterization of West Nile virus associated with multifocal retinitis in patients from southern India. *Int J Infect Dis [Internet]. Elsevier* 16(1):e53–9. Available at: <http://www.ijidonline.com/article/S120197121100213X/fulltext> [cited 2021 Mar 28]
- Smith SA, Waters NJ (2019) Pharmacokinetic and pharmacodynamic considerations for drugs binding to alpha-1-acid glycoprotein [Internet]. *Pharm Res Springer New York LLC* : 30. Available at <https://www.ncbi.nlm.nih.gov/pmc/articles/PMC7089466/>
- Smith DB, Simmonds P, Jameel S, Emerson SU, Harrison TJ, Meng XJ, et al (2014) Consensus proposals for classification of the family Hepeviridae. *J Gen Virol*
- Steinegger M, Meier M, Mirdita M, Vöhringer H, Haunsberger SJ, Söding J (2019) HH-suite3 for fast remote homology detection and deep protein annotation. *BMC Bioinform* 20(473).
- Studer G, Rempfer C, Waterhouse AM, Gumienny G, Haas J, Schwede T (2020) QMEANDisCo—distance constraints applied on model quality estimation. *Bioinformatics* 36:1765–1771
- Tang X, Yang C, Gu Y, Song C, Zhang X, Wang Y, et al (2011) Structural basis for the neutralization and genotype specificity of hepatitis E virus. *Proc Natl Acad Sci USA.* [Internet]. National Academy of Sciences 108(25):10266–71. Available at: [/pmc/articles/PMC3121834/?report=abstract](https://pubmed.ncbi.nlm.nih.gov/2121834/) [cited 2020 Oct 16]
- Thi DVL, Debing Y, Wu X, Rice CM, Neyts J, Moradpour D, et al (2016) Sofosbuvir inhibits hepatitis E virus replication in vitro and

- results in an additive effect when combined with ribavirin. *Gastroenterology* [Internet]. Elsevier, Inc 150(1):82–85.e4. <https://doi.org/10.1053/j.gastro.2015.09.011>
- Turner J, Ch'ng CL (2008) Acute hepatitis E with coexistent *Plasmodium falciparum* infection in a patient with a history of foreign travel. *Am J Case Rep* 9:252–4
- WHO (2020) Hepatitis E: key facts [Internet]. Available at <https://www.who.int/news-room/fact-sheets/detail/hepatitis-e>
- Wilson A, Ndam N, Nsangou O, Njoya M, Njouom R, Kowo M et al (2020) Seroprevalence of HEPATITIS E virus infection and factors associated in HIV infected patients in Yaoundé (Cameroon). *Open J Gastroenterol* 10:181–186
- Yang J-M, Shen T-W (2005) A pharmacophore-based evolutionary approach for screening selective estrogen receptor modulators. *Prot Struct Funct Bioinform* 59:205–220
- Zhang Y, Vermeulen NPE, Commandeur JNM (2017) Characterization of human cytochrome P450 mediated bioactivation of amodiaquine and its major metabolite N-desethylamodiaquine. *Br J Clin Pharmacol* [Internet]. Blackwell Publishing Ltd 83(3):572–83. Available at: [/pmc/articles/PMC5306493/](https://pubmed.ncbi.nlm.nih.gov/306493/) [cited 2021 Mar 28]
- Zhang S, Qu C, Wang Y, Wang W, Ma Z, Peppelenbosch MP et al (2018) Conservation and variation of the hepatitis E virus ORF2 capsid protein. *Gene Elsevier BV* 675:157–64
- Zheng Q, Jiang J, He M, Zheng Z, Yu H, Li T et al (2019) Viral neutralization by antibody-imposed physical disruption. *Proc Natl Acad Sci USA* 116(52):26933–26940

Publisher's Note Springer Nature remains neutral with regard to jurisdictional claims in published maps and institutional affiliations.

Authors and Affiliations

Borris Rosnay Tietcheu Galani^{1,2}  · **Vincent Brice Ayissi Owona**² · **Romeo Joel Guemmogne Temdie**³ · **Karoline Metzger**⁷ · **Marie Atsama Amougou**^{2,4} · **Pascal Dieudonné Djamen Chuisseu**⁵ · **Arnaud Fondjo Kouam**^{2,6} · **Marceline Ngounoue Djuidje**² · **Cécile-Marie Aliouat-Denis**⁷ · **Laurence Cocquerel**⁷ · **Paul Fewou Moundipa**²

¹ Laboratory of Applied Biochemistry, Department of Biological Sciences, Faculty of Science, University of Ngaoundere, P.O. Box 454, Ngaoundere, Cameroon

² Laboratory of Pharmacology and Toxicology, Department of Biochemistry, Faculty of Science, University of Yaounde I, P.O. Box 812, Yaounde, Cameroon

³ Laboratory of Medicinal Plants, Health, and Galenic Formulation, Department of Biological Sciences, Faculty of Science, University of Ngaoundere, P.O. Box 454, Ngaoundere, Cameroon

⁴ Research Center for Emerging and Reemerging Infectious Diseases (CREMER-IMPM), Virology Unit, P.O. Box 906, Yaounde, Cameroon

⁵ Department of Medicine, Medical and Biomedical Sciences, Higher Institute of Health Sciences, Université Des Montagnes, P.O. Box 208, Bangangte, Cameroon

⁶ Department of Biomedical Sciences, Faculty of Health Sciences, University of Buea, P.O. Box 63, Buea, South West Region, Cameroon

⁷ University of Lille, CNRS, INSERM, CHU Lille, Pasteur Institute of Lille, U1019-UMR9017-CIIL-Center for Infection and Immunity of Lille, 59000 Lille, France